A Response Climatology of Idealized Midlatitude Thermal Forcing Experiments with and without a Storm Track

KATRIN WALTER,* UTE LUKSCH, AND KLAUS FRAEDRICH

Meteorologisches Institut, Universität Hamburg, Hamburg, Germany

ABSTRACT

Several GCM studies indicate that eddy activity may have a considerable influence on the atmospheric response to midlatitude sea surface temperature anomalies. The effect of eddy activity on the atmospheric equilibrium response to idealized midlatitude thermal forcing is analyzed for an atmosphere with or without an idealized storm track. Experiments using a simplified global circulation model forced by thermal anomalies of different sign and location are discussed.

Consistent with the linear theory the geopotential height field displays a baroclinic response with a shallow low (high) somewhat downstream of the warm (cold) anomaly; farther downstream an equivalent barotropic response occurs with positive (negative) amplitude increasing with height. Eddy feedbacks have weak impact on the baroclinic part, but the equivalent barotropic response is strongly enhanced if the bandpass-filtered streamfunction tendency is in-phase with the linear geopotential height response. This is the case in an experiment with a warm anomaly near 40°N, located southwesterly of the idealized storm track. In the corresponding experiment with a cold anomaly the two patterns are out-of-phase and the equivalent barotropic response is slightly reduced. It is weakened (strengthened) if a warm (cold) anomaly is shifted about 10° poleward or equatorward relative to the idealized storm track. Midlatitude heat sources generate wave trains that extend equatorward and poleward developing large-scale correlations between the flow at remote locations (teleconnections). The space–time variability can be changed considerably by eddy feedbacks developing stronger variance for large-scale retrogressive traveling and standing waves. Partially, blocking-like events develop.

1. Introduction

Multiannual to multidecadal variability of the winter North Atlantic Oscillation (NAO) over the past half-century is associated with the North Atlantic sea surface temperature (SST). This is demonstrated by Rodwell et al. (1999) and Latif et al. (2000) analyzing ensemble simulations forced by observed SST and sea ice distributions taken from the GISST dataset (Parker et al. 1995). Together with the multiannual predictability of the North Atlantic SST patterns (Sutton and Allen 1997), one may conjecture a potential for North Atlantic and European climate prediction. However, in midlatitudes, the simulated response to SST anomalies is generally not as reproducible as the response to tropical SST forcing. In particular, the influences of the extratropical SST anomalies on the model atmosphere appear to be dependent on the model (its resolution, parameterizations, etc.), the initial atmospheric conditions, and on spatial structures of the SST anomalies (Lau 1997).

Several (high resolution) GCM experiments emphasize an equivalent barotropic response more or less downstream of a warm (cold) SST anomaly showing a ridge (trough) increasing with height (Palmer and Sun 1985; Latif and Barnett 1994). In other modeling studies the equivalent barotropic response is weaker and the near-surface geopotential response is dominated by a trough (ridge) decaying with height over the warm (cold) SST anomaly (Kushnir and Held 1996; Ting 1991, baroclinic response). The reasons for this discrepancy are still under discussion. Peng et al. (1997) found a dependence on the background circulation. Kushnir and Held (1996) suppose that the equivalent barotropic response is forced by transient eddy feedbacks and, therefore, is stronger if the storm tracks are better captured, for example, in high-resolution GCMs. Idealized experiments using different GCM background flows and idealized anomalous heat sources over the Atlantic show that the upper-level ridge response to the heating tends to weaken the zonal winds in the jet exit (Ting and Peng 1995). Thus, eddy fluxes reinforce the ridge north of the jet while it depends on the position

* Current affiliation: Max-Planck-Institut für Meteorologie, Hamburg, Germany.

Corresponding author address: Ute Luksch, Meteorologisches Institut, Universität Hamburg, Bundesstr. 55, D-20146 Hamburg, Germany.
E-mail: luksch@dkrz.de

of the heating relative to the storm track (Peng and Whitaker 1999; Bresch 1998). Therefore, the influence of the transient eddy transports, which are very sensitive to the model and experimental design, can explain the strong differences in magnitude and nature of the atmospheric responses to SST anomalies. Earlier experiments with low-resolution GCMs, which underestimate the synoptic activity in the atmosphere, show that these systems are insensitive to excitation by SST anomalies in midlatitudes (Spar 1973; Kutzbach et al. 1974; Simpson and Downey 1975). A full understanding of the nature of feedback processes participating in midlatitude air–sea interaction is still lacking. A comprehensive review on the midlatitude ocean–atmosphere coupling can be found in Frankignoul (1985) and Lau (1997).

While coupled ocean–atmosphere GCMs give extensive information on many aspects of the observed climate system (Latif 1998), simplified models of intermediate complexity provide an optimal platform for idealized experiments at low computer costs. Therefore, systematic idealized experiments of the atmospheric response to low-level heating are performed in order to document the impact of baroclinic eddy activity. The model, the experimental design, and the data analysis techniques are described in section 2. The results of a reference experiment with an idealized storm track and of the response experiments with warm and cold thermal forcing anomalies are discussed in section 3. Special emphasis lies on the impact of organized eddy activity. The results are summarized in section 4.

2. Experiment design and data analysis

A simplified global circulation model (SGCM) is used to simulate the atmospheric variability and the response to midlatitude heating or cooling. First, the model configuration is described. Then, the external forcing, the data, and the analysis techniques are introduced.

a. The model

Sensitivity experiments of intermediate length (10 yr) are performed using a SGCM (Fraedrich et al. 1998, Portable University Model of the Atmosphere, hereafter PUMA). PUMA is a modification of the SGCM of the University of Reading introduced by Hoskins and Simmons (1975) and James and Gray (1986). It is based on the dynamical core of a comprehensive GCM using the spectral transform method and a semi-implicit time-differencing scheme to integrate the primitive equations. Diabatic heating and dissipation are parameterized by Newtonian cooling and Rayleigh friction, respectively, such as proposed by Held and Suarez (1994). For our simulations PUMA is used with T21 truncation and five equally spaced sigma levels in the vertical discarding orography and moisture.

The diabatic heating Q is parameterized by the res-

toration temperature T_R, the model temperature T, and the relaxation timescale τ_R:

$$Q = \frac{T_R - T}{\tau_R}. \qquad (1)$$

The timescale τ_R is 5 days at the lowest level, 10 days at the second, and 30 days at the upper three levels. The model is set into motion as the model temperature T relaxes toward a zonally symmetric restoration temperature T_R with a large equator-to-pole gradient that decays with height. The vanishing restoration temperature difference between the North Pole and South Pole represents (perpetual) spring or autumn conditions. Note that the restoration temperature T_R is not allowed to be interpreted as a climatological mean temperature $\overline{T}$, because it represents a thermal forcing of the atmospheric circulation. Here Q is not a fixed function of space and time but is strongly controlled by the amplitude and phase of planetary waves (Shutts 1987; Marshall and So 1990).

The SGCM has been applied to study the influence of surface friction and baroclinic adjustment on the low-frequency variability in the atmosphere (James and Gray 1986; James and James 1992; James et al. 1994; Mole and James 1990; Frisius et al. 1998). Lunkeit et al. (1998) investigate the sensitivity of midlatitude eddies to baroclinicity changes due to greenhouse warming.

b. Forcing

To examine the influence of synoptic eddies on the atmospheric response to thermal anomalies experiments are conducted with and without an idealized storm track. The idealized storm track is subjected to thermal anomalies superimposed on the zonally symmetric T_R-distribution already discussed above. The climatology of the idealized storm track (Frisius et al. 1998) is referred to as reference experiment R for the response experiments with an idealized storm track. A model run with zonally symmetric conditions serves as reference experiment R_{no} for the response experiments without a storm track.

1) IDEALIZED STORM TRACK

The crucial ingredient for the existence of the Northern Hemisphere storm tracks is the mean diabatic heating in the storm track region, off the east coast of the continents (Hoskins and Valdes 1990). The diabatic heating by the warm oceans leads to enhanced baroclinicity in the atmosphere. It seems reasonable to assume that the existence and location of the storm tracks is somehow related to the existence of these strongly baroclinic regions (Chang and Orlanski 1993; Orlanski 1998). The interaction of the atmosphere with the upstream mountain chains could play an important role in providing suitable disturbances (Hoskins and Valdes 1990). Therefore, our idealized single storm track is modeled by disturbing the zonally symmetric restoration
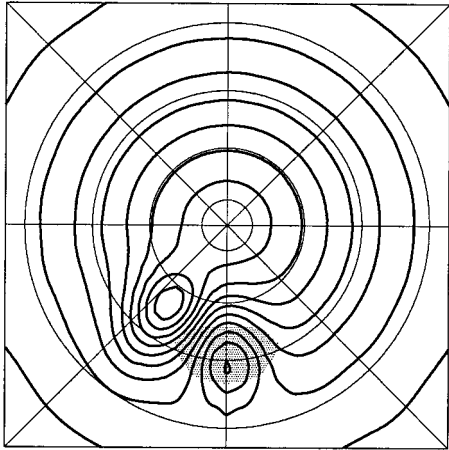
FIG. 1. Restoration temperature field at 900 hPa for the reference experiment R with the storm track generating dipole pattern (contours in 10 K). For the response experiments a T_R monopole (shaded) centered at 0°E, 41.5°N (over the warm ocean part of reference experiment dipole) is superimposed. Additional experiments are carried out in which the monopoles are shifted about 10° poleward or equatorward. The indicated latitudes are 20°, 40°, 60°, and 80°N.

temperature (T_R) field with a superimposed large-scale T_R dipole (Frisius et al. 1998), which describes the effect of a cold continent upstream and north of a warm ocean (Fig. 1). This *reference experiment with an idealized storm track* (R) exhibits a region of enhanced synoptic eddy activity downstream of the dipole pattern (Frisius et al. 1998, see also section 3a).

2) THERMAL ANOMALIES

In our sensitivity experiments we investigate the influence of baroclinic eddies on the response climatology of idealized midlatitude thermal forcing. Although little is known about the detailed heating distribution due to midlatitude SST anomalies (Frankignoul 1985), several modeling results suggest that it is shallow (Ting 1991) and almost in phase with the associated SST anomalies (Palmer and Sun 1985; Ting 1991; Kushnir and Held 1996). Therefore, we parameterize a shallow heat source superimposed on the warm pole of the dipole pattern describing the warm ocean. This shallow heat source is built with a time-constant monopole restoration temperature anomaly (T_R monopole). Its meridional and zonal extent of 2000 and 4000 km is comparable with North Atlantic SST anomalies (Weare 1977; Deser and Blackmon 1993; Luksch 1996). The horizontal distribution of the T_R monopole is Gaussian decreasing monotonically with height.

If transient eddy transports are instrumental in eliciting and maintaining a response, then the sign, magnitude, and position of the T_R monopole is important. Therefore, a warm or cold T_R monopole of different amplitude (small 8 K, medium 16 K, large 24 K) is superimposed on the center of the "warm ocean" part

of the storm track generating dipole pattern at 41.5°N (response experiments W and C, respectively, Fig. 1). Additional experiments are carried out where the monopoles are shifted about 10° poleward or equatorward relative to the center of the warm ocean part of the dipole. Finally, response experiments are conducted without the idealized storm track (response experiments W_{no} and C_{no}, monopole at 41.5°N). In the following we show the response for large amplitudes, only. The diabatic heating induced by the T_R monopoles will be further discussed in section 3b.

c. Data and data analysis

Every simulation comprises 11 yr with the first year being discarded and 10 yr are analyzed twice daily to describe the response climatology of the experiments. The equilibrium response is discussed, that is, the long-term mean minus reference experiments R and R_{no}, respectively. The transient eddies are represented by the 2.5-to-6-day bandpass-filtered 500-hPa geopotential height; a lowpass filter captures fluctuations with periods of more than 10 days (Blackmon 1976). In most cases, the stationary eddies have their largest amplitude in the upper troposphere. Therefore, we consider the long-term mean geopotential height at the 300-hPa level. The following analysis tools are employed:

A t test is performed that requires statistically independent realizations. Therefore, a special averaging scheme is employed (Blackmon et al. 1983): the first 2 months of each integration are left out, the next 3 months are taken for computing the average of the regarded variable, then the next 2 months are left out again and the average is taken over the following 3 months, etc. Thus, we obtain an ensemble of 24 statistically independent realizations, which are subject to a t test. Note that almost all features discussed in this paper are significant at a level above 99.9%.

The vertical and time mean streamfunction tendency is an indicator for the influence of transient eddies on the stationary equivalent barotropic response. Taking the vertical average of the time mean vorticity equation, several terms can be neglected and the equation reduces to a balance of divergence of the eddy vorticity flux and dissipation (Orlanski 1998):

$$-\boldsymbol{\nabla} \cdot \widehat{\overline{\mathbf{v}'\zeta'}} + \mathbf{k} \cdot \boldsymbol{\nabla} \times \widehat{\overline{\boldsymbol{F}}} = 0, \qquad (2)$$

where ζ is the vertical component of the relative vorticity, $\mathbf{v} = (u, v)$ represents the horizontal velocity vector, $\mathbf{F}$ is frictional dissipation. The primes define deviations from the long-term mean indicated by bars and the hat denotes the vertical average. The inverse Laplacian of the vorticity tendency gives the streamfunction tendency, which is considered for bandpass-filtered (synoptic eddy) forcing and the lowpass-filtered eddy forcing (>10 days) separately. The tendency due to the
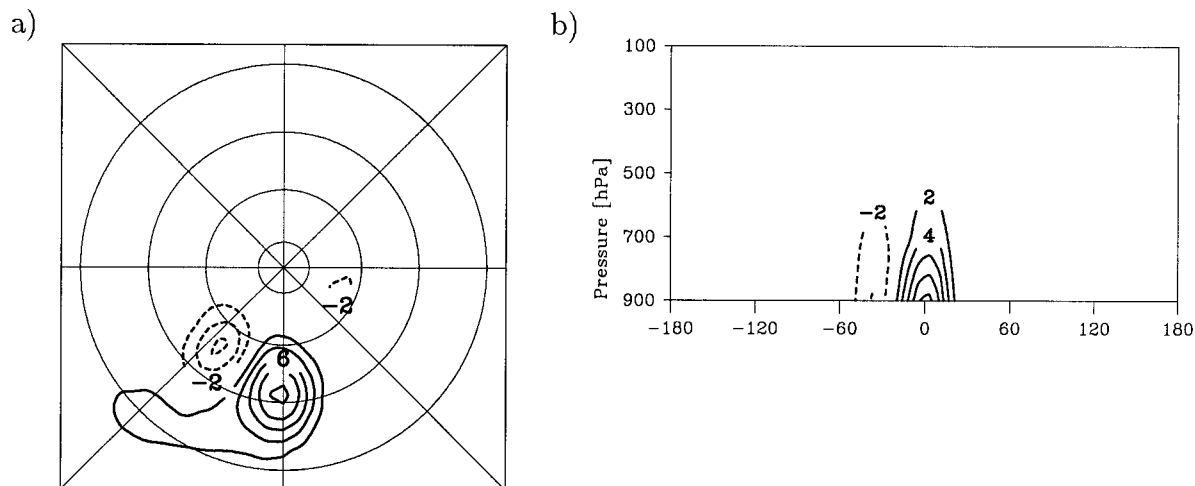
FIG. 2. Long-term mean diabatic heating rates in K day^{-1} in the reference experiment R: (a) at the 900-hPa level and (b) vertical cross section along 41.5°N. Positive (negative) values at the *x* axis in (b) denote degrees longitude east (west) of the monopole center. The zero line is not displayed.

interaction of lowpass- and bandpass-filtered eddies is small.

The maximum Eady growth rate is a measure of baroclinic instability (Eady 1949):

$$\sigma_{BI} = 0.31 \cdot f \cdot \left| \frac{\partial \mathbf{v}}{\partial z} \right| N^{-1}, \qquad (3)$$

where f is the Coriolis parameter, $\mathbf{v}$ is the time mean horizontal wind, and $N = [(g/\theta)(\partial\theta/\partial z)]^{1/2}$ is the Brunt–Väisällä frequency with the potential temperature θ. The growth rate is computed on the 700-hPa level because baroclinic development primarily operates in the lower levels of the atmosphere. It does not only depend on the meridional temperature gradient or the vertical shear of the wind but also on the static stability. A diabatic heat source would influence both vertical and horizontal temperature gradients and, therefore, the static stability as well as the vertical wind shear.

Frequency-wavenumber spectra of the barotropic (vertical mean) streamfunction describe the intensity of large-scale retrogressive traveling and standing waves versus the eastward traveling synoptic eddies (Deland 1964; Hayashi 1971, 1982). Here the global fields are approximated by a finite series of trigonometric functions (Fourier analysis) and the spectra of the sine and cosine coefficients are estimated by fitting a bivariate autoregressive process. The order of the process is given by Akaike's information criterion. The waves are split into east- and westward moving components; the coherent part can be interpreted as standing waves. Observed frequency-wavenumber spectra for the 500-hPa geopotential in 50°N show enhanced variance for the shorter eastward traveling baroclinic eddies and the longer retrogressive and standing waves (Fraedrich and Böttger 1978).

Teleconnections describe large-scale and low-fre-quency correlations between remote locations. Regarding the time series of a variable Z at a grid point i (base point), the correlation coefficients r_{ij} with the time series at every other grid point j is calculated (one-point correlation map):

$$r_{ij} = \frac{\overline{Z_i' Z_j'}}{\sqrt{\overline{Z_i'^2}}\sqrt{\overline{Z_j'^2}}}. \qquad (4)$$

The primes denote deviations from the time mean indicated by bars. Following Wallace and Gutzler (1981), we define the teleconnectivity at a certain grid point i as the maximum anticorrelation (amount of the strongest negative correlations r_{ij}) in the one-point correlation map with base point i.

3. Results

Reference and response experiments are carried out to display the influence of the eddies on the atmospheric response to midlatitude thermal forcing. First, the model climatology is introduced for the reference experiment with an idealized storm track (R, section 3a), followed by a discussion of the atmospheric response to diabatic heating and cooling monopoles (section 3b).

a. Reference experiment: A single storm track

The single storm track simulation representing the case of *enhanced* eddy activity requires changes of the zonally symmetric restoration temperature (T_R) distribution, which is referred to as the case of *reduced* eddy activity. An idealized large-scale anomaly T_R dipole is superimposed on the zonally symmetric T_R-field to incorporate the effect of a cold continent upstream of a warm ocean (Fraedrich et al. 1998; Frisius et al. 1998). This can also be inferred from the diabatic heating rates excited by this

a)

b)

c)

d)
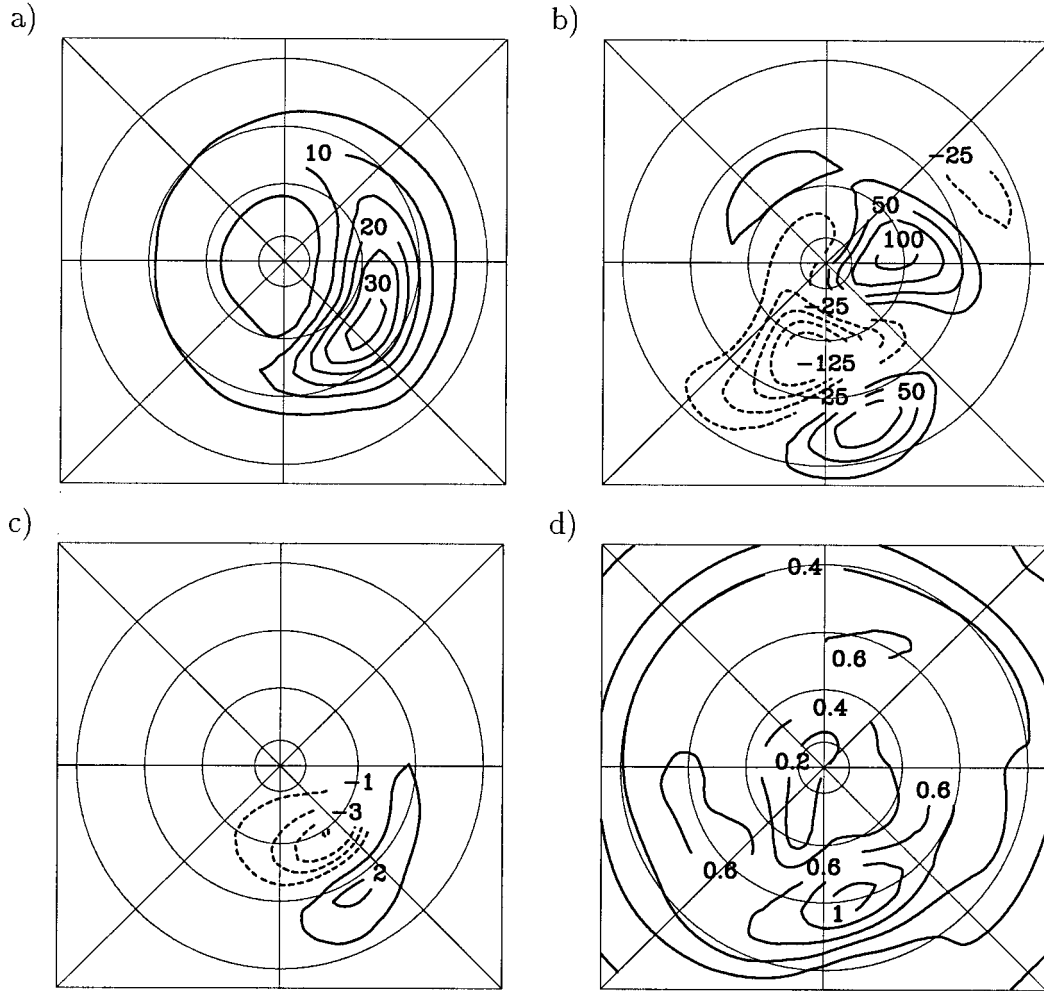
FIG. 3. Reference experiment R: (a) transient eddies (standard deviation of bandpass-filtered 500-hPa geopotential in gpm), (b) stationary eddies (long-term mean 300-hPa geopotential minus zonal mean, in gpm), (c) streamfunction tendency due to bandpass-filtered transient eddies in $m^2 s^{-2}$, and (d) maximum Eady growth rate at 700 hPa in day^{-1}. The zero line is not displayed in (b) and (c).

forcing, which show a negative shallow diabatic heat source northwest of a positive one (Fig. 2). So the heat sources are almost in phase with the T_R dipole itself. For the sake of simplicity, the meridian passing through the center of the warm ocean part of the storm track generating dipole is attributed to 0° longitude.

The climatology of the reference experiment agrees, in a qualitative sense, with observations. The atmosphere is stably stratified with the static stability increasing with latitude and reaching its maximum at the uppermost level (above the tropopause). The zonally averaged mean surface pressure shows nearly the right magnitude for the subtropical highs and the midlatitude troughs in the Northern Hemisphere. The climatological temperature at 900-hPa reveals a warm anomaly in the southwestern sector upstream of the dipole. Further details are noted.

1) TRANSIENT AND STATIONARY EDDIES (FIG. 3)

The standard deviation of bandpass-filtered 500-hPa geopotential is underestimated by a factor two in comparison with the North Atlantic wintertime storm track (Roeckner et al. 1992, and Fig. 3a) but its pattern is of realistic elongation. The stationary response of the 300-hPa geopotential (minus its zonal mean, Fig. 3b) shows low (high) values near the cold (warm) part of the anomaly dipole. Equatorward and poleward extending stationary wave trains emerge.

The streamfunction tendency due to synoptic eddies shows a dipole structure with a negative tendency north and a positive tendency south of the storm track axis (Fig. 3c). Thus, the eddies act to accelerate the westerlies in the middle of the storm track but also deflect them poleward at the exit of the storm track, which is in agreement with observations; only the simulated
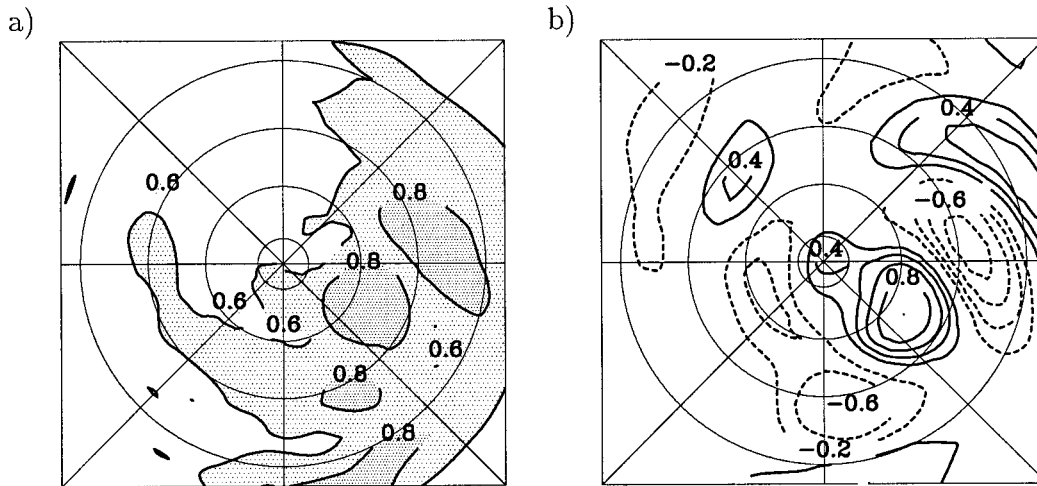
FIG. 4. Reference experiment R: (a) teleconnectivity (>0.8 shaded heavily, 0.6–0.8 shaded lightly), and (b) local correlations of monthly mean 300-hPa geopotential (base point: 52.6°N, 56.3°E). The zero line is not displayed in (b).

magnitude is much smaller (Orlanski 1998). The streamfunction tendency is in phase with the bandpass-filtered eddy momentum fluxes (Fraedrich et al. 1998), which are underestimated by the model (Roeckner et al. 1992). Note that the bandpass filter introduced by Blackmon (1976) does not capture fluctuations with periods longer than 6 days. If longer periods (up to 12 days) were captured the streamfunction tendency would show sim-

ilar patterns but with a stronger magnitude (Frisius et al. 1998; Orlanski 1998).

The climatological zonal wind maximum of 35 m s^{-1} is comparable with comprehensive GCM results or observations. The jet is located downstream of the warm part of the T_R dipole. The maximum Eady growth rate shows that the baroclinicity is strongest in the jet region (Fig. 3d).
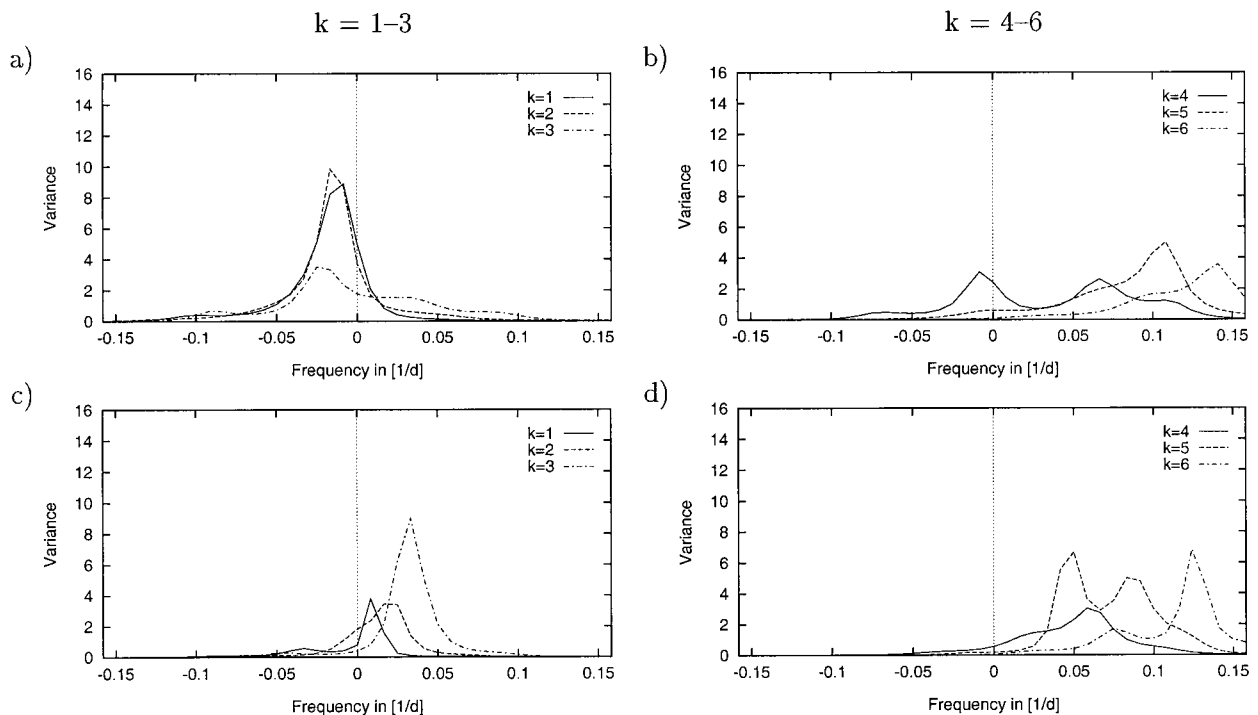
FIG. 5. Frequency–wavenumber spectra of barotropic streamfunction (63.7°–36.0°N average, in 10^{12} m^4 s^{-2}) for (a), (b) reference experiment R and (c), (d) reference experiment R$_{no}$ (without an idealized storm track). Positive (negative) frequencies represent eastward (westward) traveling waves; (a), (c) zonal wavenumbers 1–3 and (b), (d) zonal wavenumbers 4–6.

a)

b)
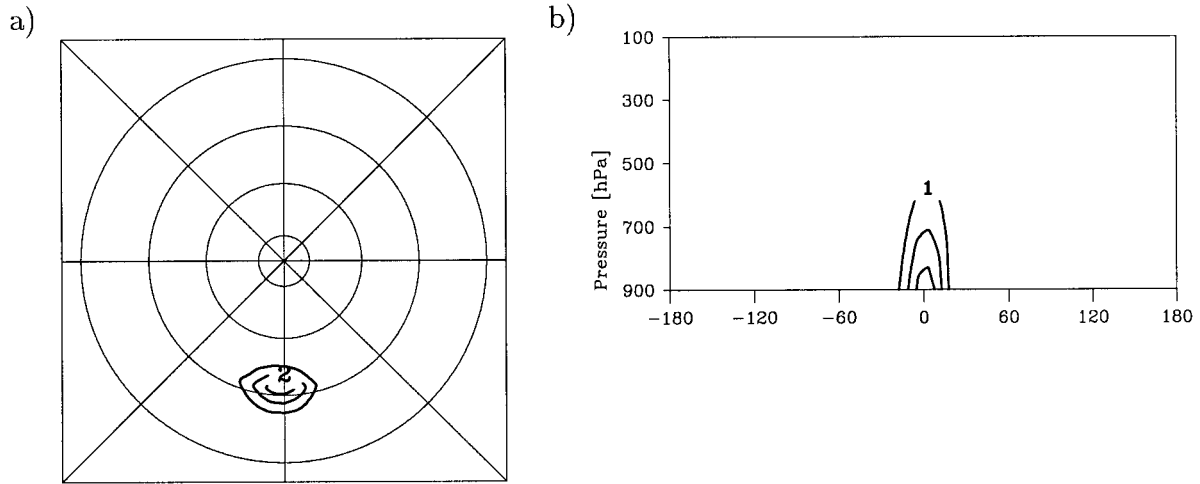
FIG. 6. Long-term mean diabatic heating rates in K day^{-1} due to a warm monopole at 41.5°N: (a) at the 900-hPa level and (b) vertical cross section along 41.5°N. Positive (negative) values at the x axis in (b) denote degrees longitude east (west) of the monopole center. The zero line is not displayed.

a)

b)

c)

d)
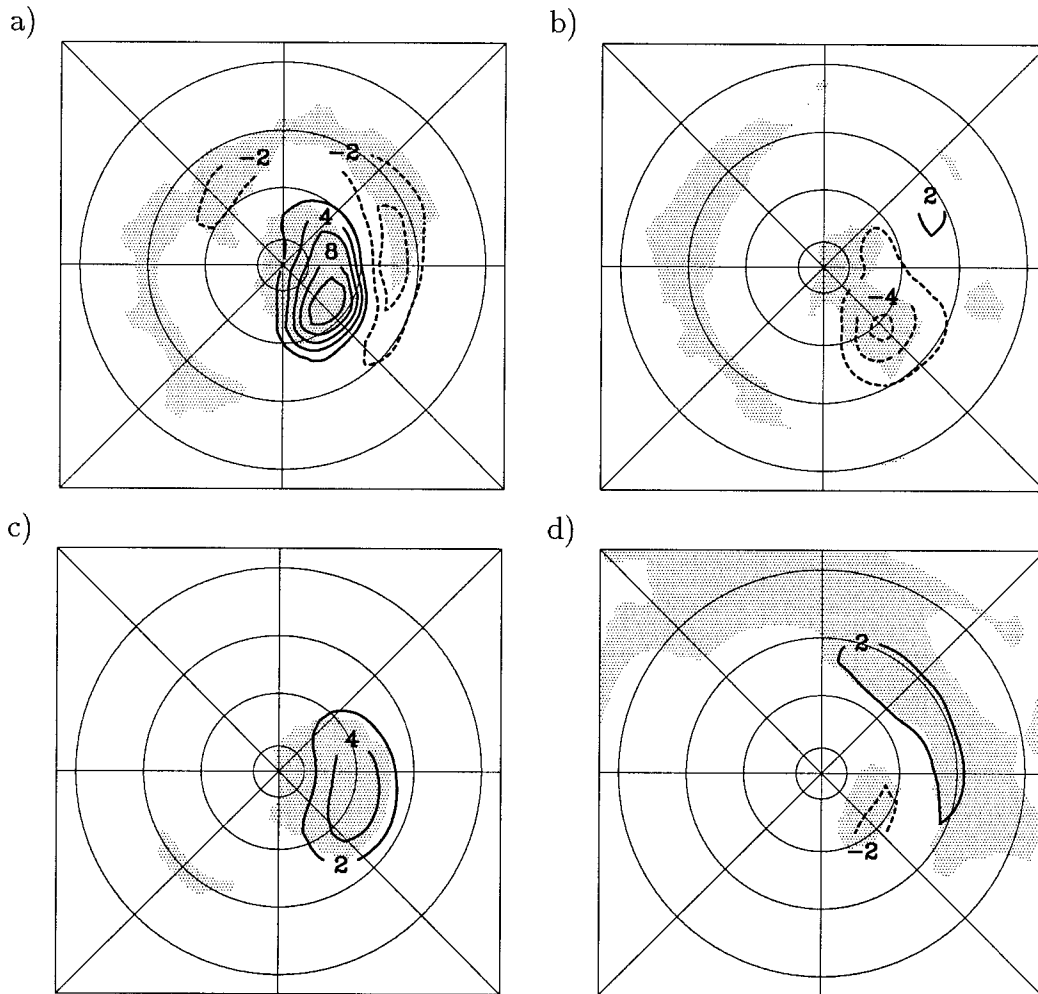
FIG. 7. Response of the standard deviation of bandpass-filtered 500-hPa geopotential height in gpm: (a) experiment W, (b) experiment C, (c) experiment W$_{no}$, and (d) experiment C$_{no}$. The zero line is not displayed. The shading indicates significance above the 99.9% level.

a)

b)

c)

d)
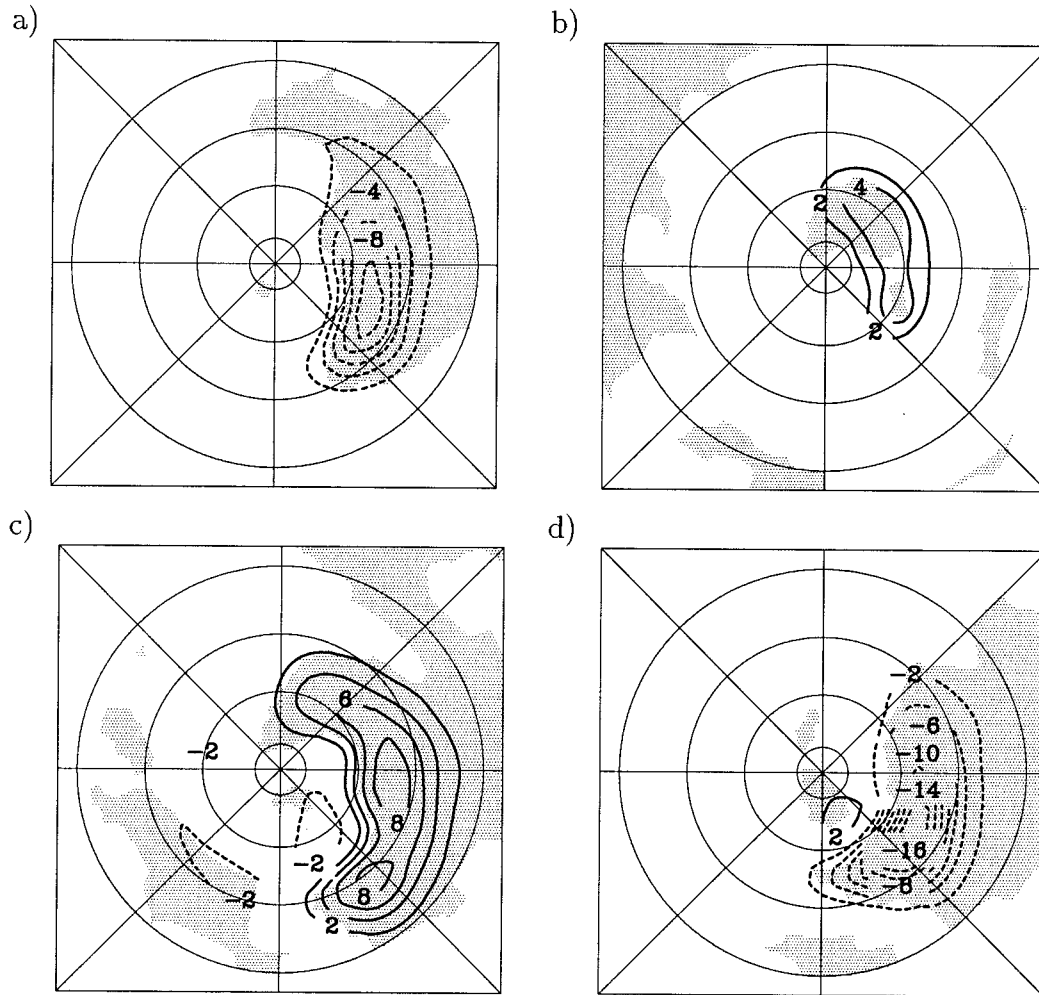
FIG. 8. Same as Fig. 7a,b but monopoles are shifted about 10° (a, b) poleward and (c, d) equatorward.

2) TELECONNECTIVITY (FIG. 4)

The stationary wave trains noted above are related to standing waves. They represent low-frequency oscillations in the spatial shape of teleconnection patterns. The teleconnectivity in the monthly mean 300-hPa height fields shows four centers of action (Fig. 4a) that can be identified by a one-point correlation map. The correlation map for the base point 52.6°N, 56.3°E (Fig. 4b) describes a wave-train-like pattern having the shape of a poleward arc running parallel to the stationary wave pattern (Fig. 3b).

3) SPACE–TIME VARIABILITY (FIG. 5)

The frequency–wavenumber spectra of the barotropic streamfunction show large-scale low-frequency retrogressive traveling and standing waves (wavenumbers 1–3, Fig. 5a), which are strong compared to the eastward traveling synoptic-scale eddies (wavenumbers 4–6, Fig. 5b). However, in the zonal symmetry experiment (R_{no},

Figs. 5c,d) eastward propagating synoptic eddies of wavenumbers 3–6 dominate (which are not organized) whereas retrogressive traveling waves are negligible.

b. Response experiments: Warm and cold monopole

Sensitivity experiments are carried out to investigate the impact of eddy feedbacks on an atmosphere responding to midlatitude thermal forcing. Therefore, the response to positive and negative thermal forcing in terms of T_R monopoles is analyzed for an atmosphere whose variability is enhanced by an idealized storm track or reduced in the zonally symmetric case. A warm or cold T_R monopole (at different positions) is embedded in the warm ocean part of the T_R dipole and in the zonally symmetric T_R distribution. The T_R monopoles induce shallow diabatic heating monopoles (Fig. 6) being almost in phase with the restoration temperature anomaly. The heating is linear about sign and amplitude of the T_R monopole. A large T_R monopole of 24 K located at

a)

b)

c)

d)
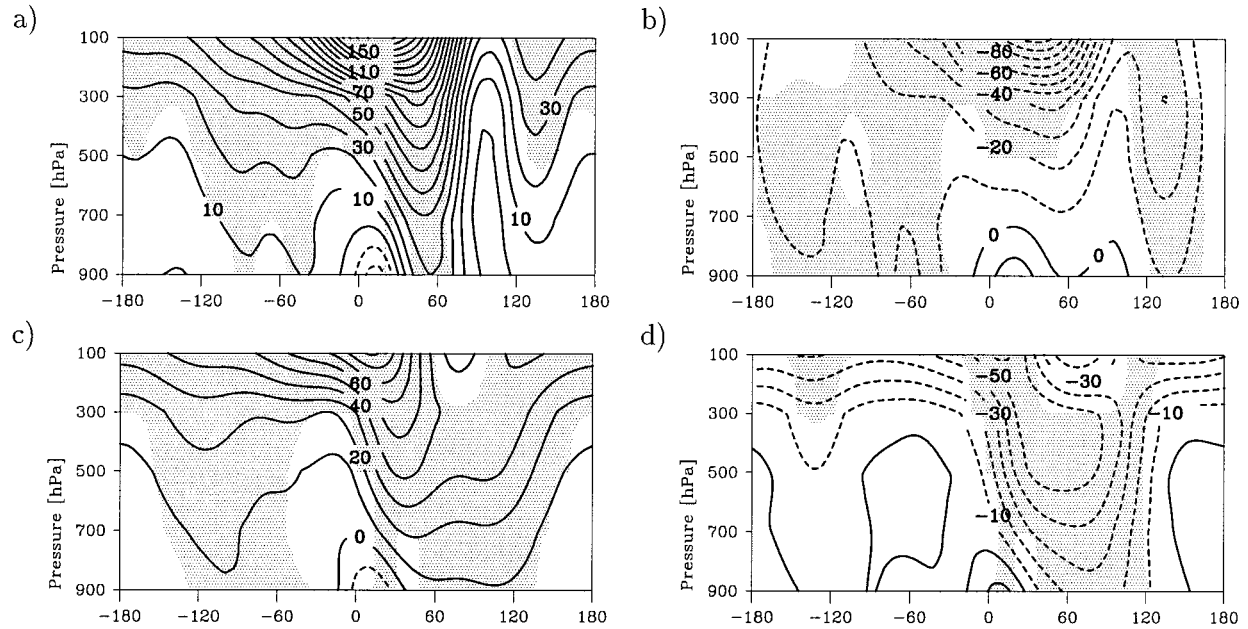
FIG. 9. Vertical cross sections of the geopotential height response along 47.1°N in gpm: (a) experiment W, (b) experiment C, (c) experiment W_{no}, and (d) experiment C_{no}. The shading indicates significance above the 99.9% level.

41.5°N corresponds to a maximum diabatic heating rate of about 3.5 K day^{-1} in the lowest model level. There is no extra heating (or cooling) due to the superposition of the monopole and the dipole pattern; the heating rates induced by monopole and dipole superpose almost linearly. Thus, if the response is significantly different in corresponding experiments with or without a T_R dipole, this difference must be due to internal dynamics. Note that the total diabatic heating comprises both sensible and convective heat exchange, and, therefore, the amplitude of the T_R monopole has to be larger than the SST anomalies in more comprehensive GCM experiments (Ting 1991; Kushnir and Held 1996).

First, the response climatology for transient and stationary eddies is described in terms of differences to the corresponding reference experiments R and R_{no}, respectively (with an idealized storm track or zonally symmetric). Teleconnectivity and space–time variability follow later.

1) TRANSIENT AND STATIONARY EDDIES (FIGS. 7–13)

The presence of a warm monopole (response experiment W, with idealized storm track) leads to a poleward shift of the storm track (Fig. 7a) whereas a cold monopole (experiment C, with idealized storm track) decreases the synoptic activity (Fig. 7b). In the zonally symmetric setting, a warm monopole (W_{no}) induces a weak increase of synoptic eddy activity (Fig. 7c) downstream and poleward of the anomalous forcing. A similar experiment with a cold monopole (C_{no}) shows a weak

decrease poleward of the monopole and a weak increase farther downstream (Fig. 7d). Furthermore, the storm track is weakened (strengthened) by a poleward (equatorward) displacement of the warm monopole and an equatorward (poleward) displacement of its cold counterpart (Fig. 8).

Consistent with the linear theory (e.g., Hoskins and Karoly 1981), the near-field response to midlatitude heating is baroclinic showing a warm lower-level trough and an upper-level ridge east of a warm monopole (Figs. 9a,c). For midlatitude cooling a positive geopotential height anomaly at the surface develops together with an upper-level negative height anomaly (Figs. 9b,d). The strength of the surface pressure response near the forcing varies almost linearly with the forcing and remains almost independent of synoptic eddy activity (Fig. 10). Downstream and north of the warm (cold) monopole a positive (negative) geopotential anomaly develops with equivalent barotropic vertical structure (Figs. 9 and 11). Regarding the upper-tropospheric geopotential height (Fig. 11), the equivalent barotropic response in experiment W (C) is strongly enhanced (slightly reduced) in comparison to the no-storm-track experiment W_{no} (C_{no}). This indicates an influence of eddy feedbacks, which is supported by the fact that the strength of the response also depends on the position of the anomalous forcing relative to the idealized storm track: If the warm monopole is displaced about 10° equatorward or poleward the equivalent barotropic response is strongly reduced (Figs. 12a,c). For cold monopoles the equivalent barotropic response is stronger in the displacement experiments (Figs. 12b,d). Note that for the equatorward shift
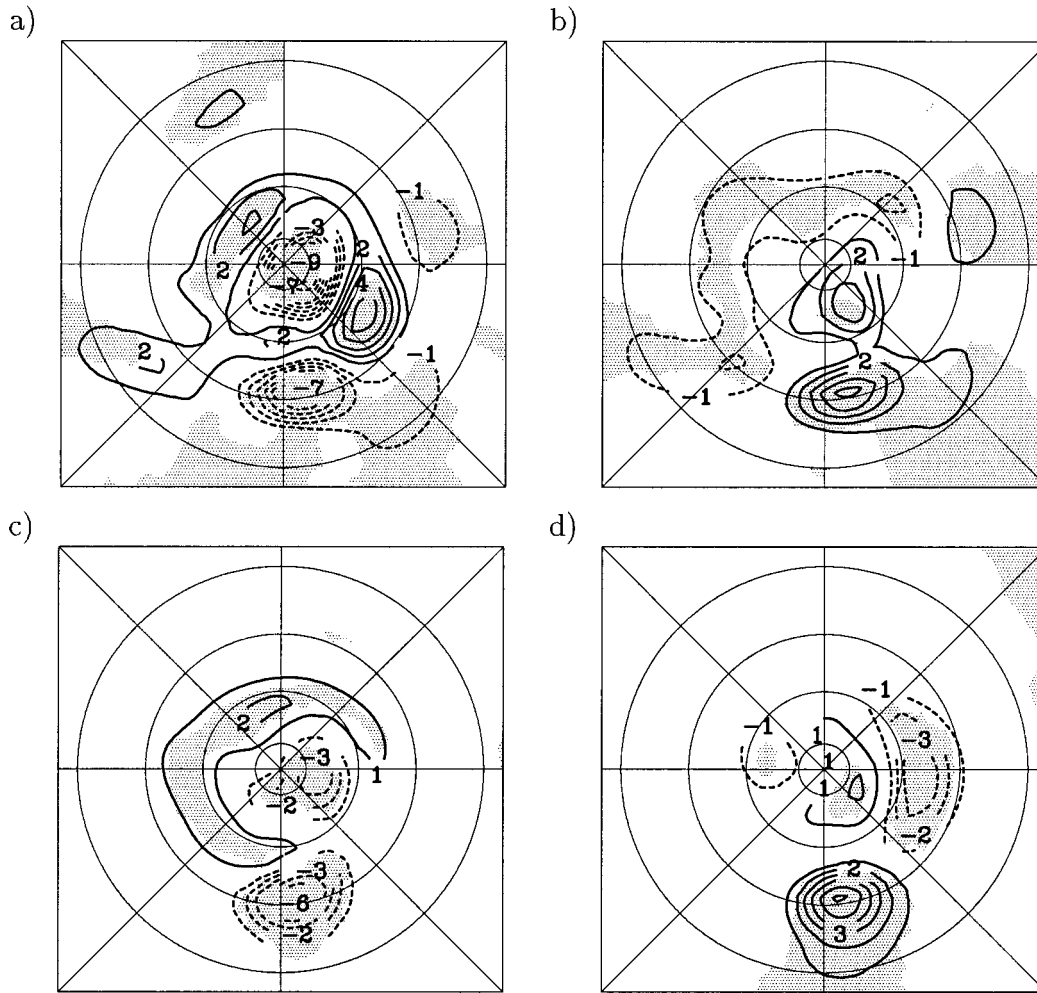
FIG. 10. Surface pressure response in hPa: (a) experiment W, (b) experiment C, (c) experiment W_{no}, and (d)
experiment C_{no}. The zero line is not displayed. The shading indicates significance above the 99.9% level.

of a warm or cold monopole a marked secondary equivalent barotropic response pattern is observed farther downstream that is anticorrelated; that is, a warm monopole creates a negative geopotential anomaly located at the position of the downstream high in experiment W.

The vertical and time mean streamfunction tendency also displays the important role of transient (especially synoptic) eddies for the strength of the equivalent barotropic response. The tendency due to bandpass-filtered transient eddies in the experiment W (warm monopole and idealized storm track, Fig. 13a) reflects the poleward shift of the storm track (Fig. 7a). The positive and negative tendencies in the reference experiment R (Fig. 3c) are shifted to the northeast in the response experiment W. The maximum is almost in phase with the equivalent barotropic geopotential response (Fig. 11a) and the synoptic eddies enhance the downstream ridge compared to the no-storm track experiment (Fig. 11c). The low-pass-filtered eddies produce a tendency toward a (north-

westerly) displacement of the downstream high (not shown). The streamfunction tendency induced by the interaction of bandpass- and lowpass-filtered eddies is negligible (not shown). In the experiment with a cold monopole and an idealized storm track, C, the streamfunction tendency induced by synoptic eddies is out-of-phase with the equivalent barotropic geopotential response (Figs. 13b and 11b). Therefore, the equivalent barotropic response is weak. In the experiments with reduced eddy activity, W_{no} and C_{no}, the streamfunction tendency by bandpass-filtered eddies is very weak ($< \pm 0.5$ m^2 s^{-2}, not shown).

The westerlies in the jet exit are slowed down in experiments W and W_{no}. In the corresponding cold monopole experiments, the geopotential height response accelerates the zonal wind. The jet stream is broader, shorter, and weaker (narrower, longer, and stronger) in the experiment W (C) than in the reference case. Corresponding to the stronger geopotential height response

a)

b)

c)

d)
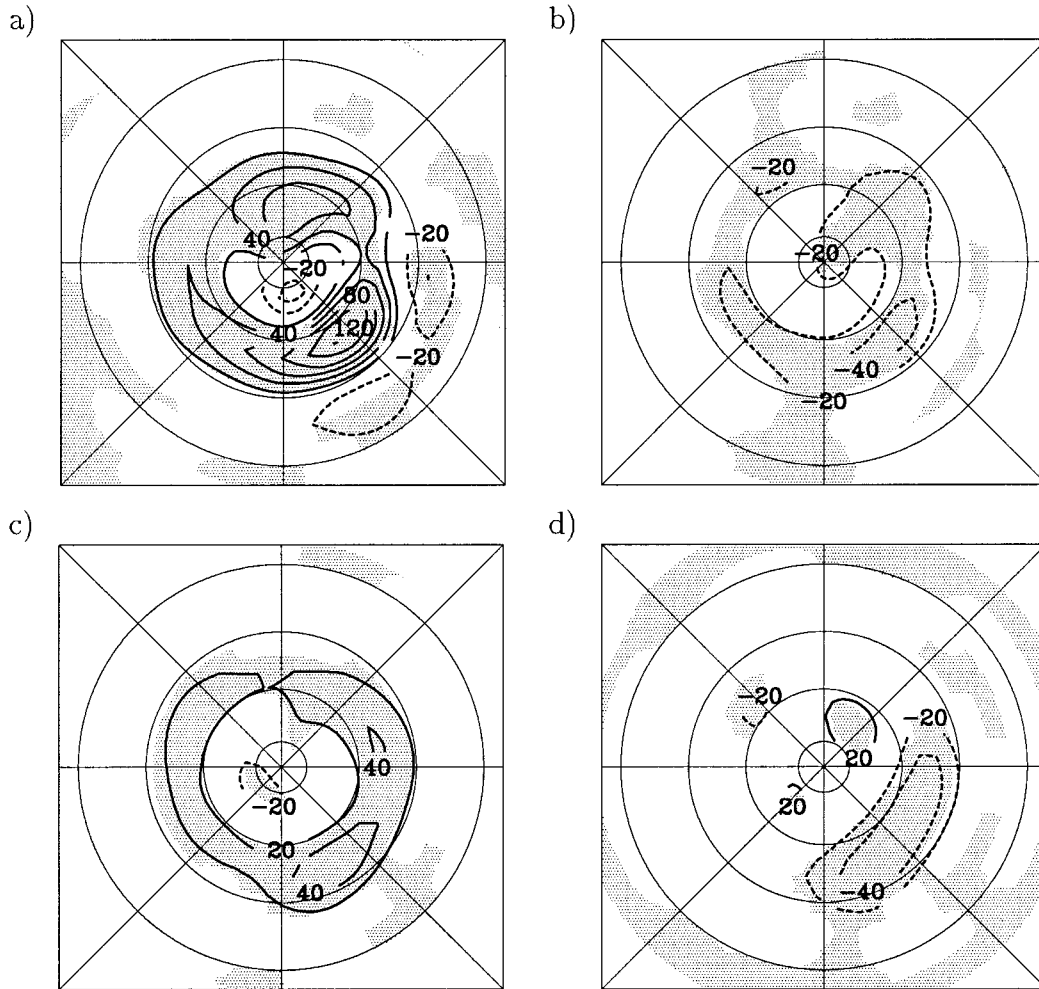
FIG. 11. The 300-hPa geopotential height response in gpm: (a) experiment W, (b) experiment C, (c) experiment W$_{no}$, and (d) experiment C$_{no}$. The zero line is not displayed. The shading indicates significance above the 99.9% level.

in experiment W the strength of the upper-level zonal wind response is also much stronger than in experiment C. This is reflected in the baroclinicity (Figs. 13c,d).

In modeling studies the strength of the equivalent barotropic response crucially depends on the model configuration (Peng et al. 1995, 1997; Kushnir and Held 1996). High-resolution models often show a stronger equivalent barotropic response than low resolution or linear models. This is probably due to the influence of the transient eddies and their feedbacks. In summarizing, the results from our response experiments with an idealized storm track are, in a qualitative sense, similar to recent high-resolution model simulations: transient eddies are instrumental in eliciting and maintaining the response (Peng et al. 1995, 1997; Bresch 1998) by eddy-induced feedbacks depending on the position of the SST heating relative to the storm track (Bresch 1998; Peng and Whitaker 1999). In the zonally symmetric case (without an idealized storm track) the atmospheric re-

sponse to midlatitude thermal forcing has similarities with the response characteristics of linear or coarse grid GCMs, where transient eddy activity is weak (Spar 1973; Kutzbach et al. 1974; Simpson and Downey 1975). The responses appear to be weak in these studies. However, the responses are larger if the anomalies are placed closer to the equator (Rowntree 1972; Julian and Chervin 1978; Wells 1979).

2) TELECONNECTIVITY (FIG. 14)

In the response experiment with a warm monopole and a storm track, W, six centers of action emerge that are related to two wave-train-like teleconnection patterns (Fig. 14a). Four of the centers are associated with the poleward extending wave-train-like pattern, which is also observed in the reference experiment (see section 3a and Fig. 4a). The remaining two centers are related to a wave-train-like pattern running parallel to meridi-

a)

b)

c)

d)
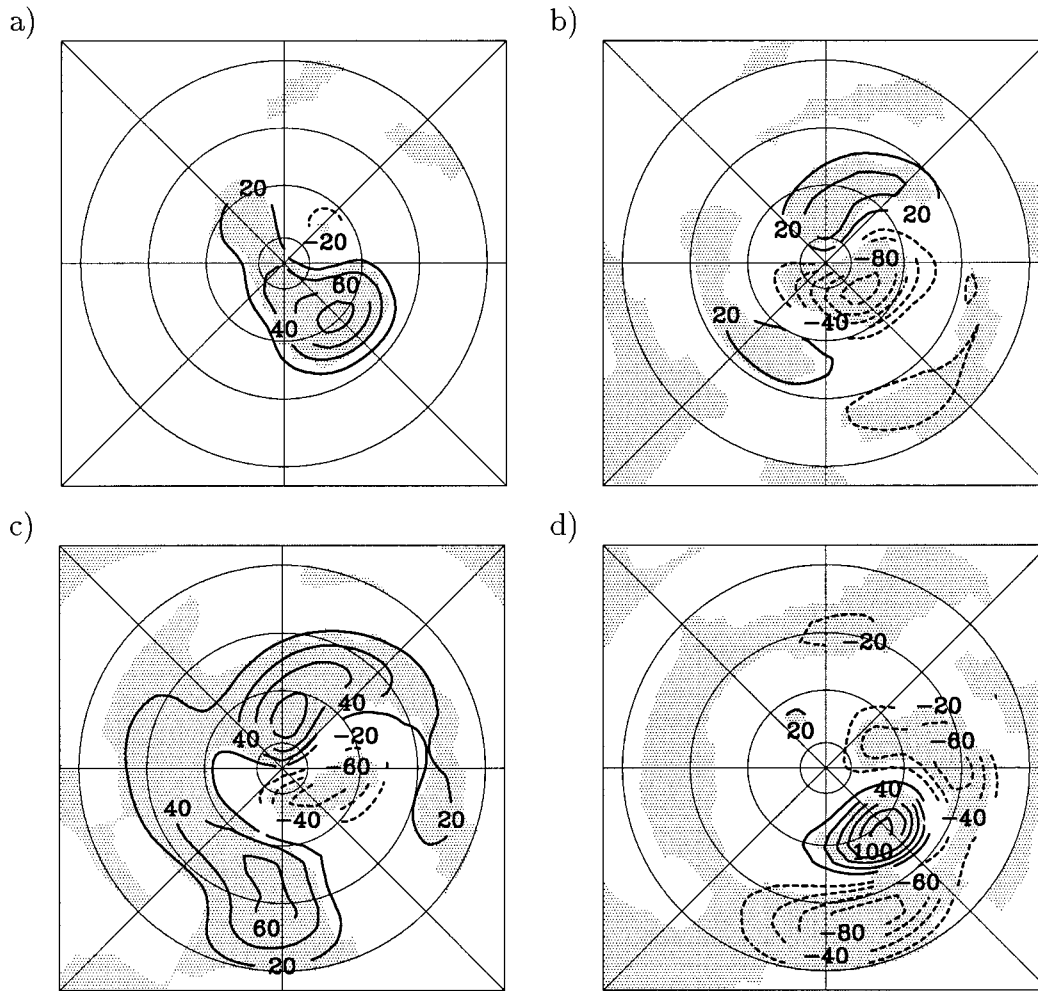
FIG. 12. Same as Fig. 11a,b but monopoles are shifted about 10° (a, b) poleward and (c, d) equatorward.

onal stationary wave trains (Fig. 11a) as can be inferred from the associated local correlations for a grid point in one of the centers (Fig. 14b). Though weak, this wave-train-like pattern is also existent in the no-storm-track experiment (W_{no}, Figs. 14c,d). In summarizing, two teleconnection patterns are induced by the storm-track-dipole and the warm monopole. In the response experiment with a warm monopole and a storm track, W, both patterns are present. They influence each other and become partially synchronized as can be seen in Fig. 14b. However, a cold monopole of the same strength does not lead to a stable teleconnection pattern (response experiment C_{no}, not shown). Therefore, experiments with cold monopoles are not further discussed.

3) SPACE–TIME VARIABILITY (FIGS. 15 AND 16)

With and without a storm track, the warm monopole response experiments show considerable changes in space–time variability. This is displayed in frequency-

wavenumber spectra and Hovmöller diagrams of the barotropic streamfunction and the 300-hPa geopotential, respectively. With a storm track, there is a strong maximum for large-scale low-frequency retrogressive traveling and standing waves (wavenumbers 1–3, Figs. 5a and 15a). This maximum is enhanced and shifted to lower frequencies if a warm monopole is included (response experiment W, Fig. 15a). The retrogressive traveling waves are negligible in the no-storm-track experiments (Fig. 15c).

The enhanced low-frequency variability of the response experiment W can be related to blocking events. This is demonstrated by a longitude-time (Hovmöller) diagram of the 300-hPa geopotential fluctuation along 52.6°N (Fig. 16a) where blocking events alternate with long lasting periods in which eastward-traveling high-frequency disturbances dominate in the storm track area. Five blocking events appear during a period of about 1200 days. Before and after that period the flow behaves as in the reference experiment (with a storm track, Fig. 16b), where retrogressive traveling geopotential anom-
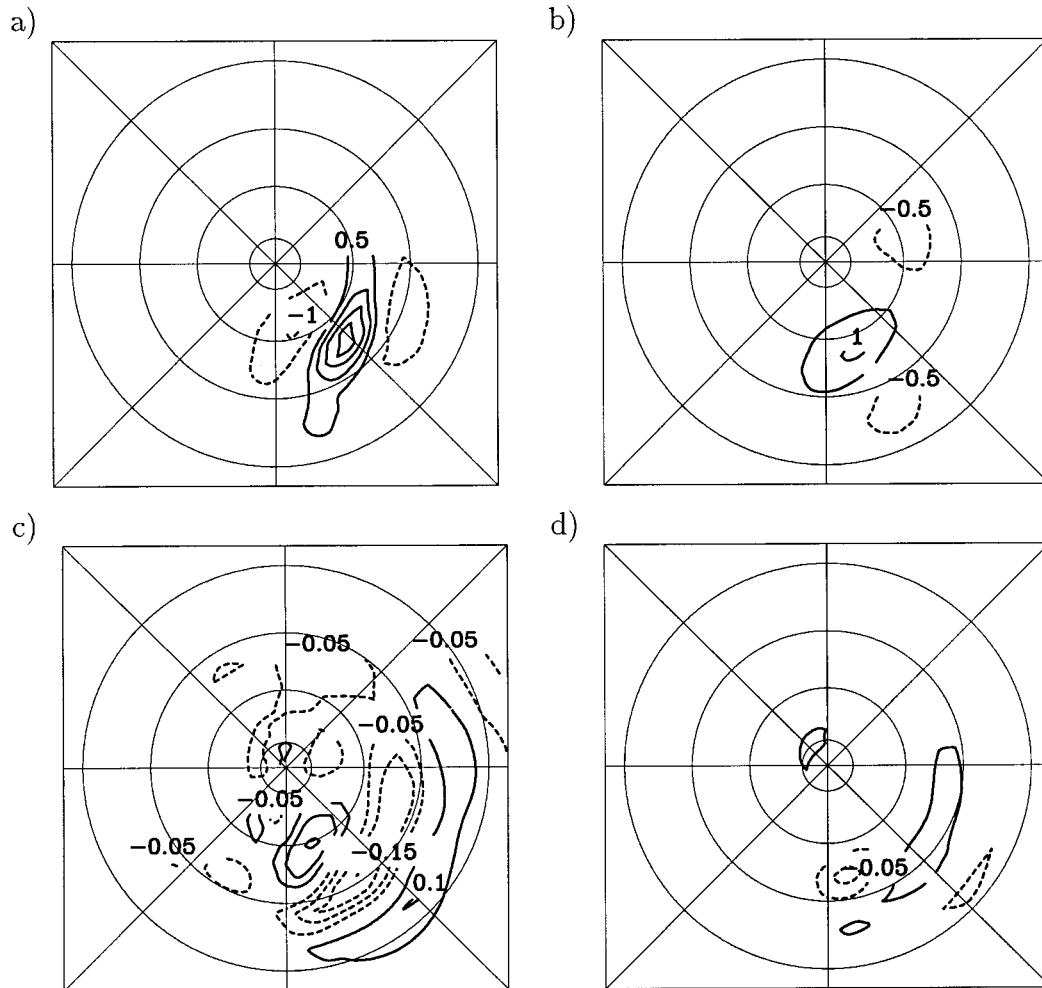
FIG. 13. Response of (a), (b) vertical mean streamfunction tendency due to bandpass-filtered transient eddies in $m^2 s^{-2}$ and (c), (d) maximum Eady growth rate at 700 hPa in day^{-1}: (a), (c) experiment W and (b), (d) experiment C. The zero line is not displayed.

alies appear almost regularly with a preferred period of about 50 days (Frisius et al. 1998) not developing such long-lasting blocking events. The latter appears to be a general pattern of the experiment W and may be related to nonlinear interactions between different space- and timescales producing low-frequency variability in the atmosphere (James and James 1992; James et al. 1994). In this sense anomalies in the real world act to bias the atmospheric circulation (Bladé 1997) toward certain flow regimes by increasing their persistence.

4. Summary

The continuing disparity between GCM response studies to midlatitude SST anomalies requires further analysis of the midlatitude ocean–atmosphere interaction (Kushnir and Held 1996). Several GCM experiments indicate that eddy activity may have a considerable influence on the atmospheric response to mid-

latitude SST anomalies. To document the effect of eddy activity, the atmospheric equilibrium response to idealized midlatitude thermal forcing is analyzed for an atmosphere with or without an idealized storm track using a simplified global circulation model (SGCM). The idealized storm track is generated by a dipole pattern superimposed on the zonally symmetric restoration temperature distribution (T_R), which represents the case of reduced eddy activity. The T_R-dipole pattern idealizes the effect of a cold continent upstream of a warm ocean (Frisius et al. 1998). A T_R monopole is included to represent the effects of warm or cold thermal forcing. Note that the diabatic heating is linear about sign and amplitude of the T_R monopole and that the heating rates induced by the T_R monopole and the T_R dipole superpose almost linearly. Sensitivity experiments are carried out to discuss the nonlinearity of the response depending on the monopole, its sign (warm or cold) and its position
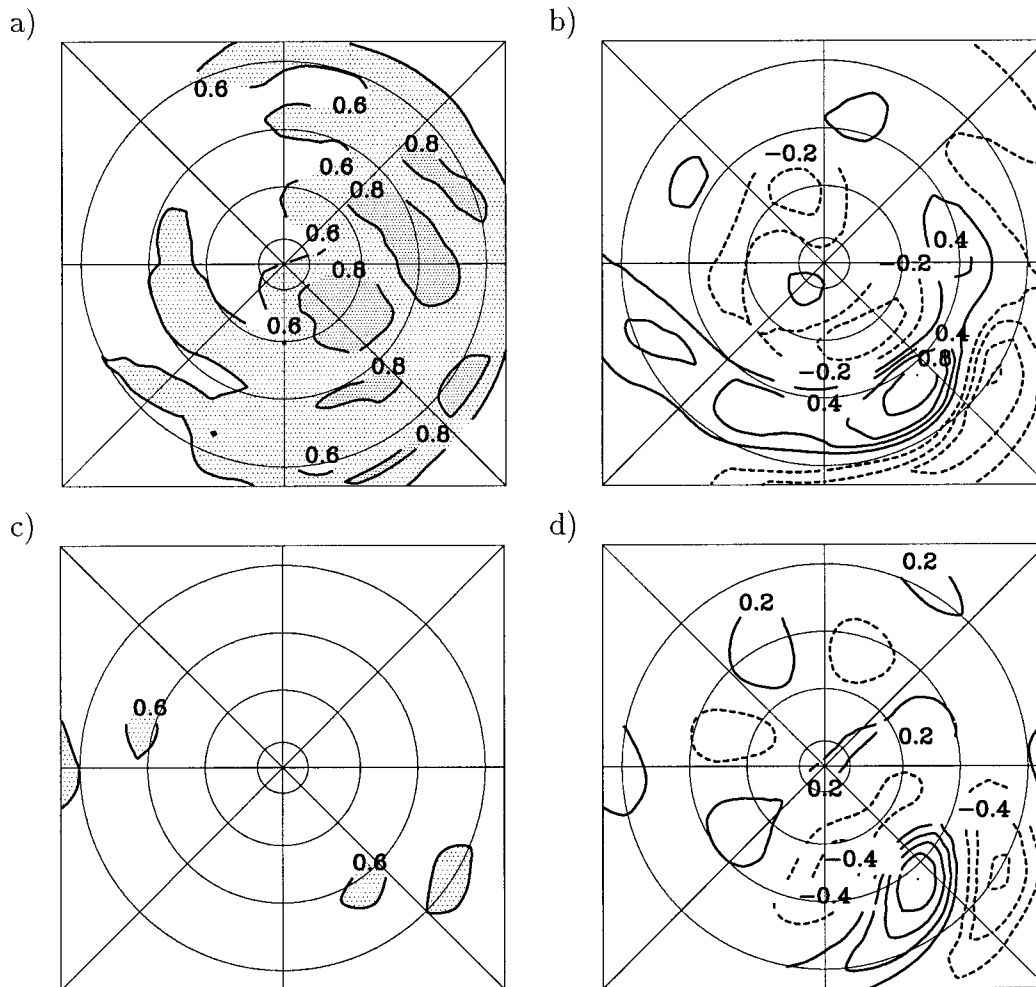
FIG. 14. (a), (c) Teleconnectivity (>0.8 shaded heavily, 0.6–0.8 shaded lightly) and (b), (d) local correlations of the monthly mean 300-hPa geopotential (base point: 36.0°N, 39.4°E). Response experiments with a warm monopole: (a), (b) with an idealized storm track (W) and (c), (d) zonally symmetric (W_no). The zero line is not displayed in (b) and (d).

relative to the idealized storm track. The following results are noteworthy.

The synoptic eddy activity migrates poleward for a warm monopole located in the middle of the warm ocean; the storm track is weakened (strengthened), if the warm monopole is shifted poleward (equatorward). A cold monopole weakens the idealized storm track; a poleward (equatorward) displacement enhances (decreases) the eddy activity. Already in the zonally symmetric setting the response is highly nonlinear.

All experiments show that the stationary geopotential response is composed of a baroclinic and an equivalent barotropic component. The baroclinic component is observed near the warm monopole with a lower-level trough and an upper-level ridge (and vice versa for the cold monopole case). It is shown that eddy feedbacks have weak impact on the low-level baroclinic trough (ridge). The equivalent barotropic response occurs farther downstream with maximum amplitude in the upper

troposphere and positive (negative) geopotential anomalies for warm (cold) monopoles. The strong intensification (slight weakening) of the equivalent barotropic response in the experiment with a storm track plus warm (cold) monopole W (C) is consistent with the streamfunction tendency response due to synoptic eddies. The stationary equivalent barotropic response is strongly enhanced if the bandpass-filtered streamfunction tendency pattern is in phase with the linear geopotential height response (warm monopole centered at 41.5°N) and it is slightly reduced in the out-of-phase case (cold monopole centered at 41.5°N). The important role of the transient eddies in the storm track is further documented by experiments in which the forcing monopoles are displaced relative to the storm track; the response is weakened (strengthened) if the warm (cold) monopole is displaced poleward or equatorward.

The space–time variability can be modified considerably due to the eddy feedbacks; in the response ex-

k = 1–3

a)

k = 4–6

b)

c)

d)
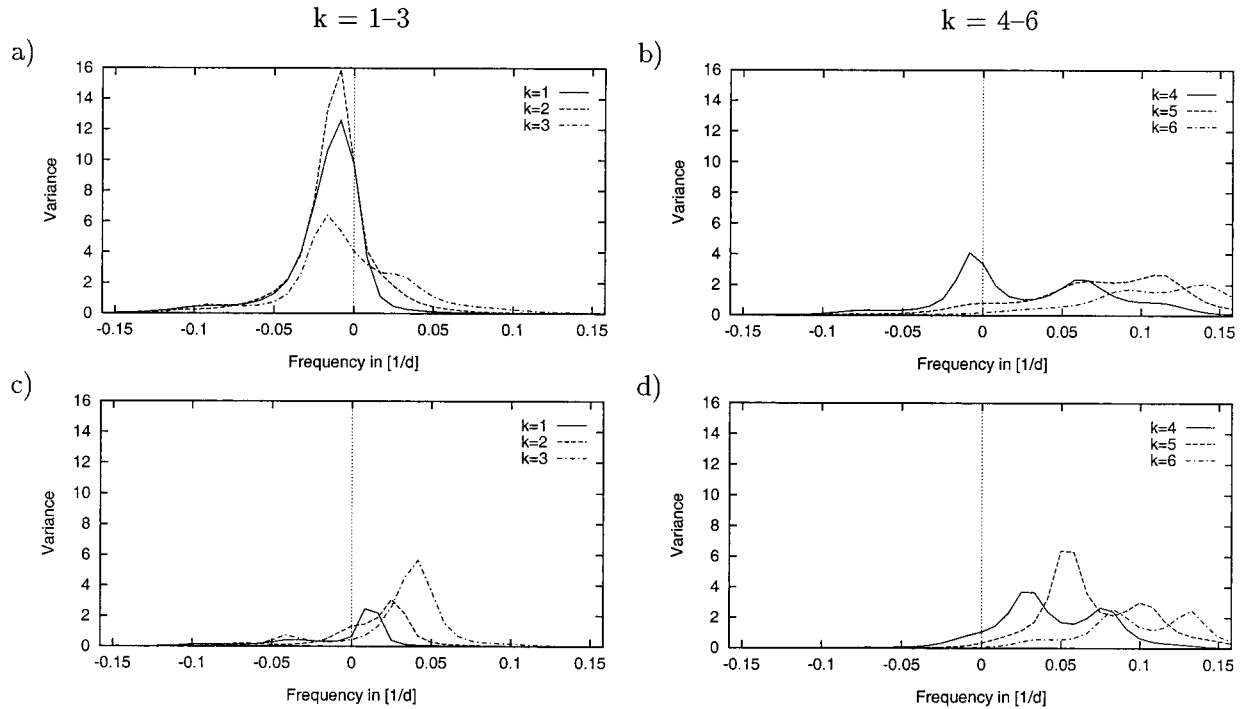
FIG. 15. Frequency–wavenumber spectra of barotropic streamfunction (63.7°–36.0°N average, in 10^{12} m^4 s^{-2}) for response experiments with a warm monopole: (a), (b) with an idealized storm track (W) and (c), (d) zonally symmetric (W_{no}). Positive (negative) frequencies represent eastward (westward) traveling waves; (a), (c) show zonal wavenumbers 1–3 and (b), (d) zonal wavenumbers 4–6.

periment W (warm monopole with an idealized storm track), the variance of large-scale retrogressive traveling and standing waves increases and, partially, blocking-like events develop. In this experiment two different teleconnection patterns are identified. These are related to wave trains induced by the warm monopole and by the storm-track-dipole, respectively. When superimposed, they influence each other and become partially correlated. There is a period where blocking-like events alternate with times when eastward traveling high-frequent disturbances predominate in the storm track area. This contrasts the reference experiment with an idealized storm track where such blocking-like events do not occur, although large-scale low-frequency retrogressive traveling and standing waves (wavenumbers 1–3) are dominant.

A large sample of earlier studies is corroborated in our analysis: in coarse grid model simulations (with reduced eddy activity) realistic midlatitude SST anomalies have weak influence on the atmospheric circulation (Frankignoul 1985). This corresponds to the results of our sensitivity experiments with reduced eddy activity (without an idealized storm track). The response experiment with an idealized storm track and a warm monopole shows an equivalent barotropic response that is more than doubled in comparison to the corresponding no-storm-track experiment. This result is comparable to high-resolution GCM studies where the eddy–mean flow interactions are better captured leading to an

enhanced equivalent barotropic response (Peng et al. 1997). Furthermore, a poleward shift of a Northern Hemispheric storm track for warm midlatitude SST anomalies was also found in several model studies (Palmer and Sun 1985; Pitcher et al. 1988; Lau and Nath 1990). In our experiments the equivalent barotropic response is highly nonlinear due to eddy forcing although the diabatic heating induced by the T_R monopole is almost linear. This adds to simulations of the atmospheric response to Pacific SST anomalies by Pitcher et al. (1988). Lunkeit and von Detten (1997) investigate the linearity of the atmospheric quasi-equilibrium response to North Atlantic SST anomalies related to interdecadal variability. Their results also indicate that the assumption of a linear correlation of the corresponding magnitudes is, in general, not valid.

This descriptive climatology of sensitivity experiments shows that eddy feedbacks play a central role for the atmospheric response to thermal forcing, which, therefore, may explain the diversity of the atmospheric responses on midlatitude SST anomalies. The equivalent barotropic response to thermal forcing strongly depends on the sign and position of the forcing relative to the region of enhanced eddy activity, whereas it appears to be roughly linear about the strength of the forcing. The latter can be inferred from experiments with reduced forcing, which are not discussed here. This point requires further examination with comprehensive GCM experiments.

a)

b)
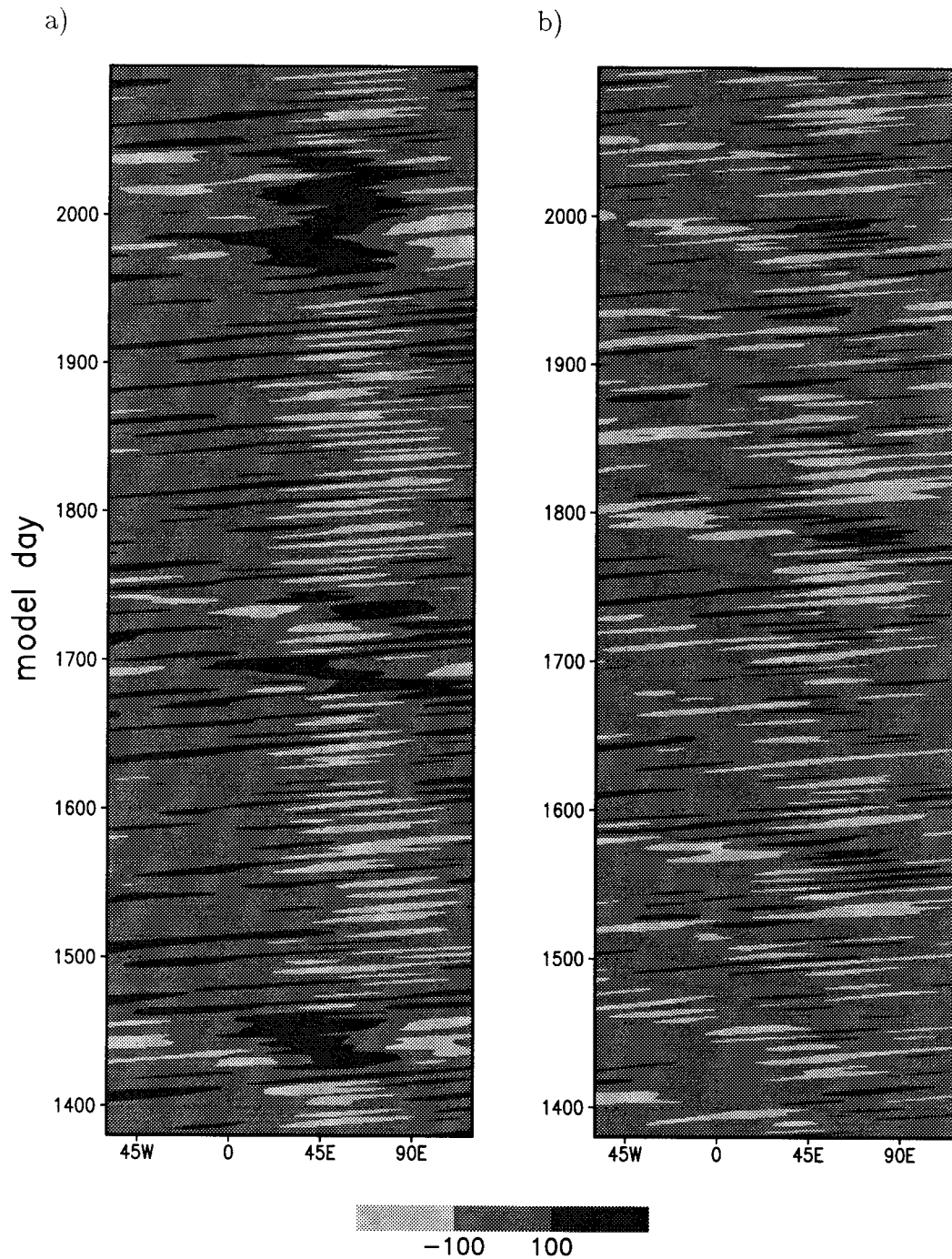
FIG. 16. Longitude–time (Hovmöller) diagram of the 300-hPa geopotential (gpm) along 52.6°N: (a) response experiment with a warm monopole (centered at 0°) and an idealized storm track (W) and (b) reference experiment with an idealized storm track (R).

In real nature SST anomalies are modified by the atmospheric flow. A positive (negative) height anomaly east of a warm (cold) SST anomaly is important for a positive feedback system in the sense of Latif and Barnett (1994). Cold continental air from the northwest cools the wintertime ocean surface due to sensible and latent heat fluxes strengthened by anomalous Ekman transport in the ocean (Luksch 1996). Studies with a comprehensive GCM are required to determine the realistic impact of baroclinic eddies on the ocean–atmosphere interaction. Moreover, further nonstationary sensitivity studies with a SGCM are planned to discuss the

physical mechanisms for the strong equivalent barotropic response together with increasing variance for low frequent large-scale retrogressive and standing waves and the blocking events. The nonstationary streamfunction tendency due to synoptic eddies in a two-storm-track experiment shows that the bandpass-filtered eddies tend to amplify the retrogressive wave pattern whereas the lowpass-filtered eddies damp it (Franzke et al. 2000). It appears that atmospheric eddy feedback is important for a notable atmospheric response to midlatitude SST anomalies and for the development of a strong ocean–atmosphere interaction.

REFERENCES

Blackmon, M. L., 1976: A climatological spectral study of the 500 mb geopotential height of the Northern Hemisphere. *J. Atmos. Sci.,* **33,** 1607–1623.

——, J. E. Geisler, and E. J. Pitcher, 1983: A general circulation model study of January climate anomaly patterns associated with interannual variation of equatorial Pacific sea surface temperatures. *J. Atmos. Sci.,* **40,** 1410–1425.

Blade, I., 1997: The influence of mitlatitude ocean/atmosphere coupling on the low-frequency variability of a GCM. Part I: No tropical SST forcing. *J. Climate,* **10,** 2087–2106.

Bresch, D. N., 1998: Coupled flow and SST patterns of the North Atlantic: A statistical and dynamical study. Dissertation 12878, ETH Zürich, 119 pp. [Available from ETH, CH-8092 Zürich, Switzerland.]

Chang, E. K. M., and I. Orlanski, 1993: On the dynamics of a storm track. *J. Atmos. Sci.,* **50,** 999–1015.

Deland, T., 1964: Travelling planetary waves. *Tellus,* **16,** 271–273.

Deser, C., and M. L. Blackmon, 1993: Surface climate variations over the North Atlantic Ocean during winter: 1900–1989. *J. Climate,* **6,** 1743–1753.

Eady, E. T., 1949: Long waves and cyclone waves. *Tellus,* **1,** 33–52.

Fraedrich, K., and H. Böttger, 1978: A wavenumber-fequency analysis of the 500-mb geopotential at 50°N. *J. Atmos. Sci.,* **35,** 745–750.

——, E. Kirk, and F. Lunkeit, 1998: Portable university model of the atmosphere. Tech. Rep. 16, Deutsches Klimarechenzentrum, 37 pp. [Available online at http://www.dkrz.de/forschung/reports-eng.html.]

Frankignoul, C., 1985: Sea surface temperature anomalies, planetary waves and air–sea feedback in the middle latitudes. *Rev. Geophys.,* **23,** 357–390.

Franzke, C., F. Lunkeit, and K. Fraedrich, 2000: Low frequency variability in a simplified atmospheric GCM: Storm track induced "spatial resonance." *Quart. J. Roy. Meteor. Soc.,* **126,** 2691–2708.

Frisius, T., F. Lunkeit, K. Fraedrich, and I. N. James, 1998: Storm-track organization and variability in a simplified atmospheric global circulation model. *Quart. J. Roy. Meteor. Soc.,* **124,** 1019–1043.

Hayashi, Y., 1971: A generalized method of resolving disturbances into progressive and retrogressive waves by space Fourier and time cross-spectral analysis. *J. Meteor. Soc. Japan,* **49,** 125–128.

——, 1982: Space-time spectral analysis and its applications to atmospheric waves. *J. Meteor. Soc. Japan,* **60,** 156–171.

Held, I. M., and M. J. Suarez, 1994: A proposal for the intercom-parison of the dynamical cores of atmospheric general circulation models. *Bull. Amer. Meteor. Soc.,* **75,** 1825–1830.

Hoskins, B. J., and A. J. Simmons, 1975: A multi-layer spectral model and the semi-implicit method. *Quart. J. Roy. Meteor. Soc.,* **101,** 637–655.

——, and D. J. Karoly, 1981: The steady linear response of a spherical atmosphere to thermal and orographic forcing. *J. Atmos. Sci.,* **38,** 1179–1196.

——, and P. J. Valdes, 1990: On the existence of storm tracks. *J. Atmos. Sci.,* **47,** 1854–1864.

James, I. N., and L. J. Gray, 1986: Concerning the effect of surface drag on the circulation of a planetary atmosphere. *Quart. J. Roy. Meteor. Soc.,* **112,** 1231–1250.

——, and P. M. James, 1992: Spatial structure of ultra-low-frequency variability of the flow in a simple atmospheric circulation model. *Quart. J. Roy. Meteor. Soc.,* **118,** 1211–1233.

——, K. Fraedrich, and I. N. James, 1994: Wave-zonal-flow interaction and ultra-low-frequency variability in a simplified global circulation model. *Quart. J. Roy. Meteor. Soc.,* **120,** 1045–1067.

Julian, P. R., and R. M. Chervin, 1978: A study of the Southern Oscillation and Walker Circulation phenomenon. *Mon. Wea. Rev.,* **106,** 1433–1451.

Kushnir, Y., and I. M. Held, 1996: Equilibrium atmospheric response to North Atlantic SST anomalies. *J. Climate,* **9,** 1208–1220.

Kutzbach, J. E., M. McClintock, and D. Suchman, 1974: Response of a general circulation model to a sea temperature pertubation. *J. Atmos. Sci.,* **31,** 857–868.

Latif, M., 1998: Dynamics of interdecadal variability in coupled ocean–atmosphere models. *J. Climate,* **11,** 602–624.

——, and T. P. Barnett, 1994: Causes of decadal climate variability over the North Pacific and North America. *Science,* **266,** 634–637.

——, K. Arpe, and E. Roeckner, 2000: Oceanic control of decadal North Atlantic sea level pressure variability in winter. *Geophys. Res. Lett.,* **27,** 727–730.

Lau, N.-C., 1997: Interactions between global SST anomalies and the midlatitude atmospheric circulation. *Bull. Amer. Meteor. Soc.,* **78,** 21–33.

——, and M. J. Nath, 1990: A general circulation model study of the atmospheric response to extratropical SST anomalies observed in 1950–79. *J. Climate,* **3,** 965–989.

Luksch, U., 1996: Simulation of North Atlantic low-frequency SST variability. *J. Climate,* **9,** 2083–2092.

Lunkeit, F., and Y. von Detten, 1997: The linearity of the atmospheric response to North Atlantic sea surface temperature anomalies. *J. Climate,* **10,** 3003–3014.

——, K. Fraedrich, and S. E. Bauer, 1998: Storm tracks in a warmer climate: Sensitivity studies with a simplified global circulation model. *Climate Dyn.,* **14,** 813–826.

Marshall, J., and D. W. So, 1990: Thermal equilibration of planetary waves. *J. Atmos. Sci.,* **47,** 963–978.

Mole, N., and I. N. James, 1990: Baroclinic adjustment in a zonally varying flow. *Quart. J. Roy. Meteor. Soc.,* **116,** 247–268.

Orlanski, I., 1998: Poleward deflection of storm tracks. *J. Atmos. Sci.,* **55,** 2577–2602.

Palmer, T. N., and Z. Sun, 1985: A modelling and observational study of the relationship between sea surface temperature in the North-West Atlantic and the atmospheric general circulation. *Quart. J. Roy. Meteor. Soc.,* **111,** 947–975.

Parker, D., C. Folland, and M. Jackson, 1995: Marine surface temperature: Observed variations and data requirements. *Climatic Change,* **31,** 559–600.

Peng, S., and J. S. Whitaker, 1999: Mechanisms determining the atmospheric response to midlatitude SST anomalies. *J. Climate,* **12,** 1393–1408.

——, L. A. Mysak, H. Ritchie, J. Derome, and B. Dugas, 1995: The differences between early and midwinter response to sea surface temperature in the northwest Atlantic. *J. Climate,* **8,** 137–157.

——, W. A. Robinson, and M. P. Hoerling, 1997: The modeled atmospheric response to midlatitude SST anomalies and its de-

pendence on background circulation states. *J. Climate,* **10,** 971–987.

Pitcher, E. J., M. L. Blackmon, G. T. Bates, and S. Munos, 1988: The effect of North Pacific sea surface temperature anomalies on the January climate of a general circulation model. *J. Atmos. Sci.,* **45,** 173–188.

Rodwell, M. J., D. P. Rowell, and C. K. Folland, 1999: Oceanic forcing of the wintertime North Atlantic oscillation and European climate. *Nature,* **398,** 320–323.

Roeckner, E., and Coauthors, 1992: Simulation of present-day climate with the ECHAM model: Impact of model physics and resolution. Max-Planck Rep. 93, Max-Planck-Institut, Hamburg, Germany, 171 pp.

Rowntree, P. R., 1972: The influence of tropical East Pacific Ocean temperatures on the atmosphere. *Quart. J. Roy. Meteor. Soc.,* **98,** 290–321.

Shutts, G. J., 1987: Some comments on the concept of thermal forcing. *Quart. J. Roy. Meteor. Soc.,* **113,** 1387–1394.

Simpson, R. W., and W. K. Downey, 1975: The effect of the warm midlatitude sea surface temperature anomaly on a numerical sim-
ulation of the general circulation model of the Southern Hemisphere. *Quart. J. Roy. Meteor. Soc.,* **101,** 847–867.

Spar, J., 1973: Some effects of surface anomalies in a global general circulation model. *Mon. Wea. Rev.,* **101,** 91–100.

Sutton, R. T., and M. R. Allen, 1997: Decadal predictability of the North Atlantic sea surface temperature and climate. *Nature,* **388,** 563–567.

Ting, M., 1991: The stationary wave response to a midlatitude SST anomaly in an idealized GCM. *J. Atmos. Sci.,* **48,** 1249–1275.

——, and S. Peng, 1995: Dynamics of the early and midwinter atmospheric responses to the northwest Atlantic SST anomalies. *J. Climate,* **8,** 2239–2254.

Wallace, J. M., and D. S. Gutzler, 1981: Teleconnections in the geopotential height field during the Northern Hemisphere winter. *Mon. Wea. Rev.,* **109,** 784–812.

Weare, B. C., 1977: Empirical orthogonal analysis of Atlantic Ocean surface temperature. *Quart. J. Roy. Meteor. Soc.,* **103,** 467–478.

Wells, N. C., 1979: The effect of a tropical sea-surface temperature anomaly in a coupled ocean–atmosphere model. *J. Geophys. Res.,* **84,** 4985–4997.